

# Speckle Reduction Approach for SAR Image in Satellite Communication

Ashkan Masoomi, Roozbeh Hamzehyan, and Najmeh Cheraghi Shirazi, *Member, IACSIT*

**Abstract**—This paper represents a novel approach to improve de-speckling in SAR images. At first, Smoothing of the coefficients of the highest wavelet sub-bands is applied on decomposed wavelet coefficients. A Gaussian low pass filter using a tours algorithm has been used to decompose the image. Then, the learning of a Kohonen self organizing map (SOM) is performed directly on the de-noised image to take out the blur. Traditional speckle reduction approaches cause artificial structures, blurred and smoothed image, although intelligent de-blurring technique captured these problems. Quantitative and qualitative comparisons of the results obtained by the new method with the results achieved from the other speckle noise reduction techniques demonstrate its higher performance for speckle reduction in SAR images.

**Index Terms**—Directional smoothing, de-blurring, de-noising, wavelets.

## I. INTRODUCTION

Imaging techniques using coherent illumination, such as laser imaging, acoustic imagery and synthetic aperture radar (SAR), which generate coherent images [1], are subject to the phenomenon of speckle noise. Speckle noise is generated due to constructive and destructive interference of multiple echoes returned from each pixel. As a result, a granular pattern is produced in the radar image which corrupts significantly the appearance of the image objects. Speckle noise can be modeled as multiplicative random noise in spatial domain [2].

Many attempts were made to reduce the speckle noise. An appropriate method for speckle reduction is one which increases the signal to noise ratio while preserving the edges and lines in the image. Generally, there are two main approaches for speckle noise removal. The first is applied before image generation which is called multi-look processing [3]. In this method the synthetic aperture is divided into some pieces. Each of these apertures is processed separately to obtain a pixel with a special along-track dimension. The N images are summed to form an

N-look SAR image. The N-look processing reduces the standard deviation of the speckle. The second approach is filtering the image using different filters [4]-[9]. Two types of filters are used for speckle reduction. Low pass filters such as mean or median generally smooth the image. The second type is adaptive filtering [4]-[5].

These filters adapt themselves to the local texture information within a box surrounding a central pixel in order to calculate a new pixel value. Adaptive filters demonstrated their superiority compared to low pass filters, since they take into account the local statistical properties of the image. Adaptive filters perform much better than low-pass smoothing filters, in preservation of the image sharpness and details while suppressing the speckle noise.

Both multi-look processing and spatial filtering reduce speckle at the expense of resolution and they both essentially smooth the image. Therefore, the amount of speckle reduction desired must be balanced with the particular application and the amount of details required.

Speckle is a phenomenon inherent in coherent imaging systems with spatial resolution greater than the wavelength. Synthetic aperture radar (SAR) is an example of such an imaging system. Due to the roughness of the imaged surface, each resolution cell will contain several scatterers, and the resulting image will have a granular appearance due to constructive and destructive interference. Speckle appears as spatially correlated, multiplicative noise that is statistically independent of the image intensity, although it is a radio-metric feature of the imaged object. The granular nature of speckled images makes them hard to interpret, both for the human eye and automated segmentation and classification algorithms [10].

The usual goal of SAR imaging is to construct a two-dimensional representation of a portion of the earth's surface (or the surface of another planetary body, e.g. the Magellan mission to Venus [6]). The radar transmits an electromagnetic pulse from a side-looking antenna and 'listens' for its return. The pulse reflects, or scatters, from targets on the ground back to a receiving antenna. The radar begins digitizing the scattered signal after a pre-defined delay after pulse transmission, which can be calculated based on the flying height and the desired swath offset to the nadir track of the platform. While moving, the antenna continuously sends and receives pulses, according to the pulse repetition frequency (PRF), to construct a 2-D array of digitized signals. These two dimensions are (a) the azimuth direction, which corresponds to the travel direction of the platform and (b) the orthogonal range direction. Figure 1 shows SAR pre-processing chain.

Manuscript received October 12, 2011; revised January 16, 2012. This work was supported in part by Islamic Azad University, Ahram Branch, Iran.

Ashkan Masoomi is with the Communication Engineering Department of Islamic Azad University, Ahram Branch, Iran. (e-mail: ashkan.masoomi@yahoo.com).

Roozbeh Hamzehyan is with the Communication Engineering Department of Islamic Azad University, Boushehr Branch, Iran. (e-mail: r\_hamzehyan@yahoo.com).

Najmeh Cheraghi Shirazi is with the Electrical Engineering Department of Islamic Azad University, Boushehr Branch, Iran. (e-mail: nch\_shirazi@yahoo.com).

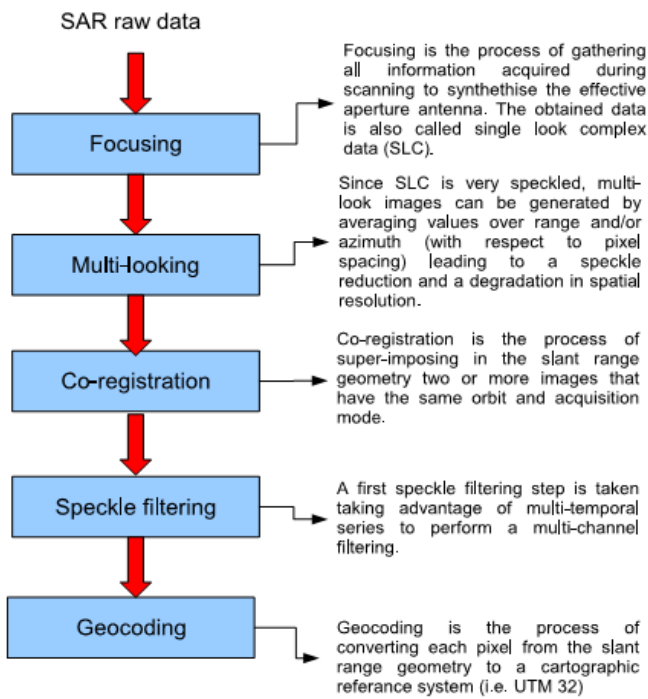


Fig. 1. SAR pre-processing chain

In many practical situations, a recorded image presents a noisy and blurred version of an original scene. The image degradation process can be adequately modeled by a linear blur and an additive noise process. Then the degradation model is described by [1]

$$g = Df + n \quad (1)$$

However, for multiplicative noise, which generally it is called speckle, we propose the follow degradation model [1]

$$g = Df \bullet s \quad (2)$$

where the vectors  $g$ ,  $f$ ,  $n$  and  $s$  represent, respectively, the lexicographically (raster scan) ordered noisy blurred image, the original image, the additive noise, and the multiplicative noise (speckle). The matrix  $D$  is the linear degradation process, and the operator “ $\bullet$ ” means element-by-element multiplication. The image de-blurring problem calls for obtaining an estimate of  $f$  given  $g$  and  $D$ . For the blind restoration problem,  $D$  is not known [2].

The true radiometric values of the image are represented by  $I$ , and the values measured by the radar instrument are represented by  $I_s$ . The speckle noise is represented by  $S$ . The parameters  $r$  and  $c$  means row and column of the respective pixel of the image. If  $S'(r,c)=S(r,c)-1$  and  $N(r,c)=I(r,c)S'(r,c)$ , we begin with a multiplicative speckle  $S$  and finish with an additive speckle  $N$  [3], which avoid the log-transform, because the mean of log transformed speckle noise is not equal to zero [1] and thus requires correction to avoid extra distortion in the restored image.

Speckle noise in SAR images is usually modeled as a purely multiplicative noise process of the form [2]

$$\begin{aligned} I_s(r,c) &= I(r,c)S(r,c) \\ &= I(r,c)[1+S'(r,c)] \\ &= I(r,c) + N(r,c) \end{aligned} \quad (3)$$

For single-look SAR images,  $S$  is Raleigh distributed (for amplitude images) or negative exponentially distributed (for intensity images) with a mean of 1. For multi-look SAR images with independent looks,  $S$  has a gamma distribution with a mean of 1. Further details on this noise model are given in [4].

A large number of techniques exist for the de-noising [5] [6] [7] and the de-blurring problems [8] [9] [10]. The image restoration problem is an ill-posed problem. Therefore, a common ingredient in all restoration approaches is that prior information is used in order to restrict the number of possible solutions (basic idea of regularization). Such prior knowledge can be stochastic (i.e., the original image is a sample of a random field) or deterministic (the high frequency energy of the restored image is bounded) in nature [11]. Regularization theory is also applied to the blind restoration problem [12].

In this paper, an original approach is developed toward both the de-noising and the de-blurring problems. Such a (nontraditional) approach for de-noising is based on the work of Mastriani and Giraldez [12]. They directly apply the Directional Smoothing (DS) filter [13] in the Bidimensional Discrete Wavelet Transform (DWT-2D) domain to reduce the presence of speckles, because the edges will be protected from blurring while smoothing. While, in order to face blur generated for the de-speckling process, the learning of a Kohonen self-organizing map (SOM) is performed directly on the de-speckled image [14]. The proposed algorithms differ from the reported results in the literature in a number of ways. Kohonen SOM, for example, is designed from a different point of view than is previously reported in the literature. In the proposed approach, each image to be used for the de-blurring problem contains both the low frequency information of the degraded image (the one which is represented by the degraded edges generated for the de-speckling process) and the corresponding high frequency information of the original image. Further improvements may be achieved by using Gaussian low pass filter and a trous algorithm for decomposition. This algorithm is well-known for using non-decimated wavelet transform which minimizes the artifact in the denoised data [15]. Shift invariancy is one of the important properties of a trous algorithm. In speckle noise reduction this property can improve the performance of the algorithm.

## II. SYNTHETIC APERTURE RADAR

Synthetic Aperture Radar (SAR) image data provide information different from that of optical sensors operating in the visible and infrared regions of the electromagnetic spectrum. SAR data consist of high-resolution reflected returns of radar-frequency energy from terrain that has been illuminated by a directed beam of pulses generated by the sensor. The radar returns from the terrain are mainly determined by the physical characteristics of the surface features (such as surface roughness, geometric structure, and orientation), the electrical characteristics (dielectric constant, moisture content, and conductivity), and the radar frequency of the sensor. By supplying its own source of illumination, the SAR sensor can acquire data day or night without regard to cloud cover. Elachi (1988) provides a technical overview

of radar wave-surface interactions and their applications to land, water, and ice phenomena in Spaceborne Radar Remote Sensing. Most other remote sensing textbooks also provide introductory material on SAR system properties and image data applications [16].

Synthetic aperture radar (SAR) satellite systems currently in operation include the European Space Agency's (ESA) European Remote Sensing Satellite 1 (ERS-1), launched July 1991, and the Japanese Earth Resources satellite (JERS-1), launched February 1992. Contacts are provided for ERS-1 data and JERS-1 data. The ERS-1 sensor operates in the C-band frequency (approx. 5.6 cm wavelength) and JERS-1 operates in the L-band frequency (approx. 23 cm wavelength). Both sensors have a nominal spatial resolution of approximately 30 m. The Canadian Space Agency plans to launch its RADARSAT in 1995. The SAR systems are now beginning to provide SAR image data on a long-term, sustained basis. The ERS-1 satellite, with a projected lifespan of three years, will be followed by an ERS-2 satellite planned to continue SAR data acquisition into the late 1990s, when advanced SAR sensors are expected to become operational as part of the Earth Observing System (EOS) [17].

The current level of experience in operational use of SAR data is very limited compared to the use of visible and infrared data acquired by the multispectral satellite sensors. Several major characteristics of SAR data taken together, however, may promote more extensive evaluation and use of SAR data for land-use and land-cover information. These characteristics include 1) the unique information of surface roughness, physical structure, and electrical conduction properties; 2) the high spatial resolution; 3) the 24-hour, all-weather data-acquisition capability; and 4) the now-realizable long-term continuity of the data that enables repetitive (seasonal) coverage of major global land regions [18]. Figure 2 shows linear model of observation SAR system.

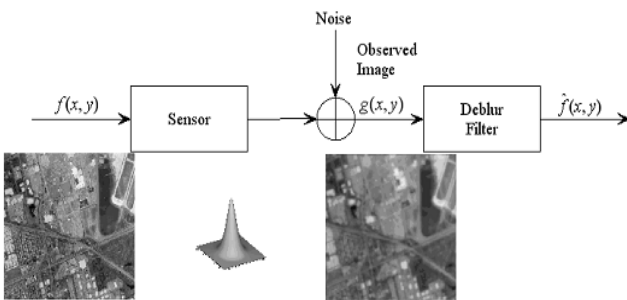


Fig. 2. Linear model of observation system

### III. DIRECTIONAL SMOOTHING

#### A. Bi-Dimensional Discrete Wavelet Transfer

In this section, some of the aspects of the WT and of the Over Complete Wavelet Transform (OCWT) will be very briefly discussed. For a more exhaustive study, [19] must be consulted.

The WT proposes the study of a complex phenomenon, dividing it into different simpler pieces [20].

$$Wf[n, a^j] = \sum_{m=0}^{N-1} f[m] \psi_j^*[m-n] \quad (4)$$

being  $f$  the discrete signal of length  $N$  and  $\psi_j$  a discrete wavelet atom,  $n$  the space coordinate,  $j$  a the resolution and  $j$  the number of iteration. This means projecting it in a particular function space in which it is located by measuring its degree of similarity with each basic function. In a WT, the basic functions come from dilations and translations of a “mother wavelet”,  $\psi$ , localized in both, time and frequency.

$$\psi_j[n] = \frac{1}{\sqrt{a^j}} \psi\left(\frac{n}{a^j}\right) \quad (5)$$

Therefore, each term of the basis allows the representation of the signal at a given scale and so the WT can focus on structures with a “zooming” procedure [21]. In 2D, a wavelet basis is constructed with separable products of a scaling function and a wavelet. Three wavelets are then defined, each of them extracting details at different orientations.

Since Sveinsson *et al.* [14] directly apply the Enhanced-Lee filter in the Bi-dimensional Discrete Wavelet Transform (DWT-2D) domain to reduce the presence of speckles. We use the DS [13], because the edges will be protected from blurring while smoothing. The experimental results demonstrate that DS is better than Enhanced-Lee filter in all the carried out experiments. Therefore, we begin decomposing the speckled SAR image into four wavelet subbands: Coefficients of Approximation (CA), and speckled coefficients of Diagonal Detail (CDDs), Vertical Detail (CVDs), and Horizontal Detail (CHDs), respectively. We apply DS within each high subband, and reconstruct a SAR image from the modified wavelet coefficients, that is to say, despeckled coefficients of Diagonal Detail (CDDd), Vertical Detail (CVDd), and Horizontal Detail (CHDd), respectively, as shown in Figure 1, where: IDWT-2D is the inverse of DWT-2D. Based on Equation (1) SmoothShrink does not need log-transform [13].

#### B. Theory of Directional Smoothing

To protect the edges from blurring while smoothing, a directional averaging filter must be applied. Spatial averages  $d(r, c; \Theta)$  are calculated in several directions as [22]

$$d(r, c; \Theta) = \frac{1}{N_\Theta} \sum_{k \in W_\Theta} \sum_{l \in W_\Theta} x(r-k, c-l) \quad (6)$$

And a direction  $\Theta^*$  is found such that  $|x(r, c) - d(r, c; \Theta^*)|$  is minimum, where  $x$  is the respective detail sub-band. Then

$$d(r, c) = d(r, c; \Theta^*) \quad (7)$$

Gives the desired result for the suitably chosen window  $W$ ,  $N_\Theta$  is the number of directions, and  $k$  and  $l$  depends on the size of such windows (kernel) [14].

The DS filter has a speckle reduction approach that performs spatial filtering in a square-moving window defined as kernel, and is based on the statistical relationship between the central pixel and its surrounding pixels as shown in Figure 3.

The size of the filter window can range from 3-by-3 to 33-by-33, with an odd number of cells in both directions. A larger filter window means that a larger area of the image will

be used for calculation and requires more computation time depending on the complexity of the filter's algorithm. If the size of filter window is too large, the important details will be lost due to over smoothing. On the other hand, if the size of the filter window is too small, speckle reduction may not be very effective. In practice, a 3-by-3 or a 7-by-7 filter window usually yields good results in the cases under study [23].

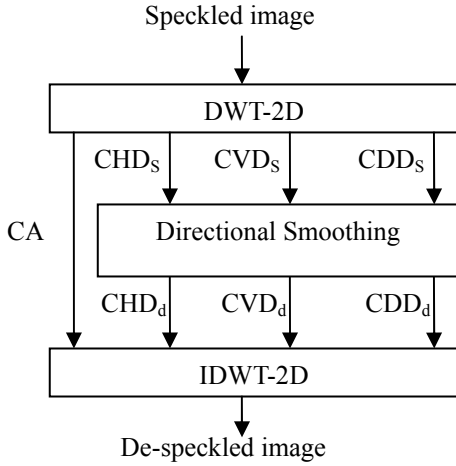


Fig. 3. Smoothing of Coefficients in wavelet domain

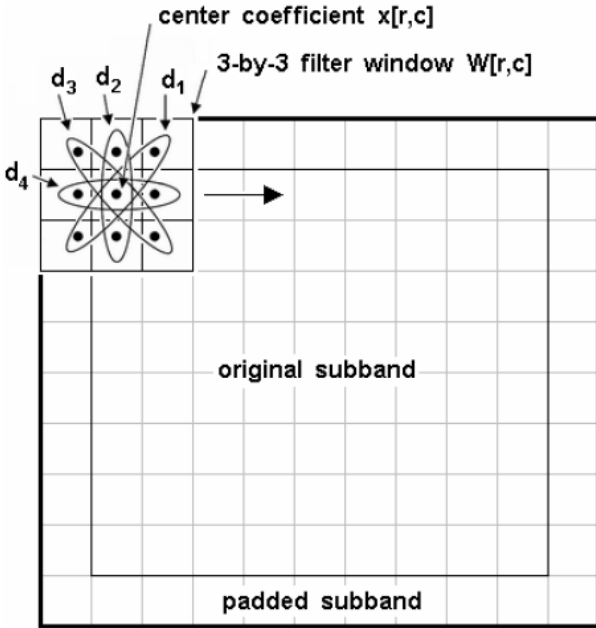


Fig. 4. 3-by-3 filter window on a sub-band

DS performs the filtering based on either local statistical data given in the filter window to determine the noise variance within the filter window, or estimating the local noise variance using the effective equivalent number of looks (ENL) of the image under study. The estimated noise variance is then used to determine the amount of smoothing needed for each sub-image. The noise variance obtained from the local filter window is more applicable if the backscatter of an area is constant (flat and homogeneous) [12].

Most simple nonlinear thresholding rules for wavelet based de-noising assume that the wavelet coefficients are independent [11] [13]. However, wavelet coefficients of

natural images have significant dependencies. In this paper, we will consider the dependencies between the coefficients and their neighbors in detail. The Smooth Shrink do not assume the independence of wavelet coefficients, because, It is based on the DS algorithm, which keeps in mind the incidence of the neighboring elements by means of the employing of a mask, which can be observed in the algorithm that is detailed next.

#### IV. SELF-ORGANIZATION MAP

Researches on neurobiology have shown that centers of diverse activities as thought, speech, vision, hearing, lie in specific areas of the cortex and these areas are ordered to preserve the topological relations between information's while performing a dimensionality reduction of the representation space. Such organization led Kohonen to develop the SOM algorithm [24]. This kind of competitive neural network is composed of one or two dimensional array of processing elements or neurons in the input space. All these neurons receive the same inputs from external world. Learning is accomplished by iterative application of unlabeled input data. As training process, the neurons evolve in the input space in order to approximate the distribution function of the input vectors. After this step, large-dimensional input vectors are, in a sense, projected down on the one or two-dimensional map in a way that maintains the natural order of the input data. This dimensional reduction could allow us to visualize and to use easily, on a one or two-dimensional array, important relationships among the data that might go unnoticed in a high-dimensional space.

The model of SOM used in our application is a one dimensional array of  $n$  nodes. To each neuron  $N_i$ , a weight vector  $w_i = (w_{i1}, w_{i2}, \dots, w_{ij})^t \in R^p$  is associated [25].

During learning procedure, an input vector  $x \in R^p$  randomly selected among vectors of the training set, is connected to all neurons in parallel. The input  $x$  is compared with all the neurons in the Euclidean distance sense via variable scalar weight  $w_{ij}$ . At the  $k$ th step, we assign the vector  $x$  to the winning or leader neuron  $N_l$  if:

$$\|x - w_l^{[k]}\| = \min_i \|x - w_i^{[k]}\| \quad (8)$$

All the neurons within a certain neighborhood around the leader participate in the weight-update process. Considering random initial values for  $w_i^{[0]}$ ,  $i, (0 \leq i \leq n)$ , this learning process can be described by the following iterative procedure:

$$w_i^{[k+1]} = w_i^{[k]} + H_{li}^{[k]}(x^{[k]} - w_i^{[k]}) \quad (9)$$

The lateral interactions among topographically close elements are modeled by the application of a neighborhood function or a smoothing Kernel defined over the winning neuron [12]. This Kernel can be written in terms of the Gaussian function

$$H_{li}^{[k]} = \alpha^{[k]} \exp\left(-\frac{d^2(l, i)}{2(\sigma^{[k]})^2}\right) \quad (10)$$

where  $d(l, i) = \|l - i\|$  is the distance between the node  $l$  and  $i$  in the array  $\sigma^{[k]}(t)$  is the learning-rate factor and  $\sigma^{[k]}$  defines the

width of the Kernel at the iteration  $k$ . For the convergence, it is necessary that  $H_i^{[k]} \rightarrow 0$  when  $k \rightarrow T$ , where  $T$  is the total number of step of the process [21]. Therefore, for the first step,  $\alpha^{[k]}$  should start with a value that is close to unity, thereafter decreasing monotonically [21]. To achieve this task, we use

$$\alpha^{[k]} = \alpha^{[0]} \left(1 - \frac{k}{T}\right) \quad (11)$$

Moreover, as learning proceeds, the size of the Neighborhood should be diminished until it encompasses only a single unit. So, we applied for the width of the Kernel the monotonically decreasing function:

$$\sigma^{[k]} = \sigma^{[0]} \left(\frac{\sigma^{[T-l]}}{\sigma^{[0]}}\right)^{k/(T-l)} \quad (12)$$

The ordering of the map occurs during the first steps, while the remaining steps are only needed for the fine adjustment of the weight values.

The learning process is performed directly on the real image to be de-blurred. An input vector is filled with the grey levels of the pixels of the image (see Figure 5, 6). Therefore, each neuron has rows-by-columns weights allowing locating it in the input space. At each step, the weights are modified according to Equation (12). Experiments have shown that this training strategy provides as good results as an ordered image scanning process while spending less processing time.

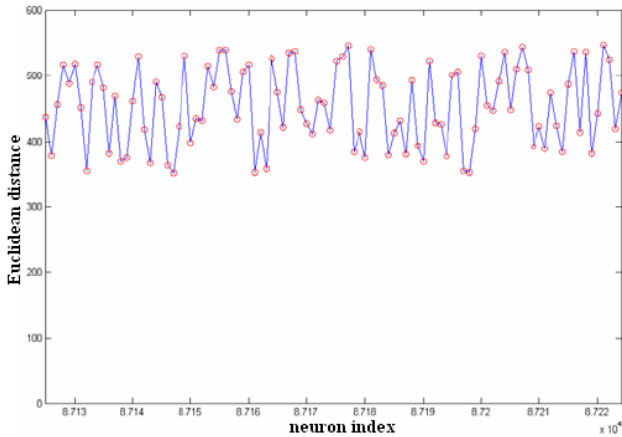


Fig. 5. The distance graph between the 100 neurons of the SOM before learning.

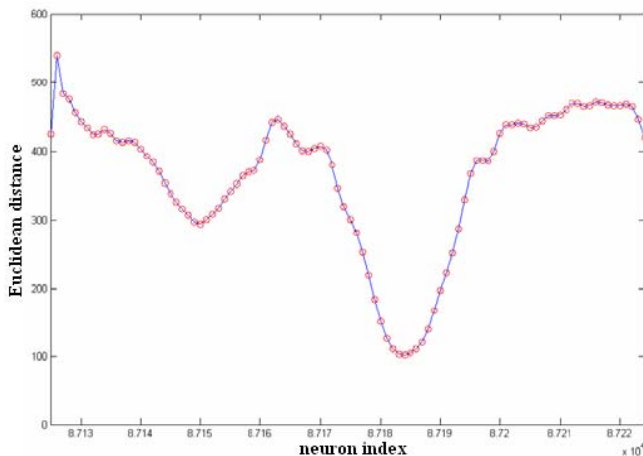


Fig. 6. The distance graph between neurons obtained after learning.

## V. ASSESSMENT PARAMETERS FOR DESPECKLING

In this work, the assessment parameters that are used to evaluate the performance of speckle reduction are Noise Variance, Mean Square Difference, Noise Mean Value, Noise Standard Deviation, Equivalent Number of Looks, Deflection Ratio, and Pratt's figure of Merit [26], [27].

### A. Noise Mean Value (NMV), Noise Variance (NV), and Noise Standard Deviation (NSD)

NV determines the contents of the speckle in the image. A lower variance gives a "cleaner" image as more speckle is reduced, although, it not necessarily depends on the intensity. The formulas for the NMV, NV and NSD calculation are

$$NMV = \frac{\sum_{r,c} I_d(r,c)}{R * C} \quad (13)$$

$$NV = \frac{\sum_{r,c} (I_d(r,c) - NMV)^2}{R * C} \quad (14)$$

$$NSD = \sqrt{NV} \quad (15)$$

where R-by-C pixels is the size of the de-speckled image  $I_d$ . On the other hand, the estimated noise variance is used to determine the amount of smoothing needed for each case for all filters.

### B. Mean Square Difference (MSD)

MSD indicates average square difference of the pixels throughout the image between the original image (with speckle)  $I_s$  and  $I_d$ , see Fig. 4. A lower MSD indicates a smaller difference between the original (with speckle) and de-speckled image. This means that there is a significant filter performance. Nevertheless, it is necessary to be very careful with the edges. The formula for the MSD calculation is [28]

$$MSD = \frac{\sum_{r,c} (I_s(r,c) - I_d(r,c))^2}{R * C} \quad (16)$$

### C. Equivalent Numbers of Looks (ENL)

Another good approach of estimating the speckle noise level in a SAR image is to measure the ENL over a uniform image region [1]. A larger value of ENL usually corresponds to a better quantitative performance. The value of ENL also depends on the size of the tested region, theoretically a larger region will produce a higher ENL value than over a smaller region but it also tradeoff the accuracy of the readings. Due to the difficulty in identifying uniform areas in the image, we proposed to divide the image into smaller areas of 25x25 pixels, obtain the ENL for each of these smaller areas and finally take the average of these ENL values. The formula for the ENL calculation is

$$ENL = \frac{NMV^2}{NSD^2} \quad (17)$$

The significance of obtaining both MSD and ENL measurements in this work is to analyze the performance of the filter on the overall region as well as in smaller uniform regions [29].

D. Deflection Ratio (DR)

A fourth performance estimator used in this work is the DR proposed by H. Guo et al (1994), [30]. The formula for the deflection calculation is

$$DR = \frac{1}{R * C} \sum_{r,c} \left( \frac{I_d(r,c) - NMV}{NSD} \right) \quad (18)$$

The ratio DR should be higher at pixels with stronger reflector points and lower elsewhere. In H. Guo et al’s paper, this ratio is used to measure the performance between different wavelet shrinkage techniques. In this paper, the ratio approach to all techniques after de-speckling in the same way [27] is applied.

E. Pratt’s Figure of Merit (FOM)

To compare edge preservation performances of different Speckle reduction schemes, the Pratt’s figure of merit is adopted [31] defined by

$$FOM = \frac{1}{\max\{\hat{N}, N_{ideal}\}} \sum_{i=1}^{\hat{N}} \frac{1}{1 + d_i^2 \alpha} \quad (19)$$

where  $\hat{N}$  and  $N_{ideal}$  are the number of detected and ideal edge pixels, respectively,  $d_i$  is the Euclidean distance between the  $i_{th}$  detected edge pixel and the nearest ideal edge pixel, and  $\alpha$  is a constant typically set to 1/9. FOM ranges between 0 and 1, with unity for ideal edge detection.

The de-blurring task consists in using the Equation (15) over the image. For each iteration, the corresponding input vector  $x$  is compared with all the neurons using Equation (14). The winning neuron, the one which leads to the smallest distance, gives the class of the winner pixel in which iteration. However, before any de-blurring task, we have to calibrate the map in order to associate the label mean or edges to each neuron.

Assuming that the input vector  $x_0 = (0, \dots, 0)$  should represent an image setting on an identical mean value, it is very useful to define the distance graph representing the Euclidean distance in the rows-by-columns-dimensional space between the point  $x_0$  and all the neurons. Such a graph is given in Figure 3 and Figure 4 respectively before and after learning for a 512- by-512-neuron network [32].

Both figures show that the maximal distance between two successive cells is smaller after learning than before. We show only 100 of 512x512 neurons around the winner. We can deduce that, after learning, neurons that are topologically close in the array are close in the input space too [33].

VI. EXPERIMENTAL RESULTS

Here, besides our approach, we present a set of experimental results using one ERS SAR Precision Image (PRI) standard of Buenos Aires area. For statistical filters employed along, i.e., Median, Lee, Kuan, Gamma-Map, Enhanced Lee, Frost, Enhanced Frost [13] Wiener [11], DS [13] [14] and Enhanced DS (EDS) [12], we use a homomographic speckle reduction scheme [14], with 3-by-3, 5-by-5 and 7-by-7 kernel windows. Besides, for Lee, Enhanced Lee, Kuan, Gamma-Map, Frost and Enhanced Frost filters the damping factor is set to 1[11] [12]. On the other hand, the statistical filters used inside SmoothShrink

method were DS and EDS .

Figure 7(a) [12] shows a noisy image used in the experiment from remote sensing satellite ERS-2, with a 242-by-242 (pixels) by 65536 (gray levels); and the filtered images, processed by using VisuShrink (Hard-Thresholding), BayesShrink, OracleShrink, SURE-Shrink, and Smooth-Shrink techniques respectively, see Table I. All the thresholding techniques used Daubechies 15 wavelet basis and 1 level of decomposition (improvements were not noticed with other basis of wavelets) [11, 12, 13]. Besides, Figure 5 summarizes the edge preservation performance of the Smooth Shrink technique vs. the rest of the shrinkage techniques with a considerably acceptable computational complexity.

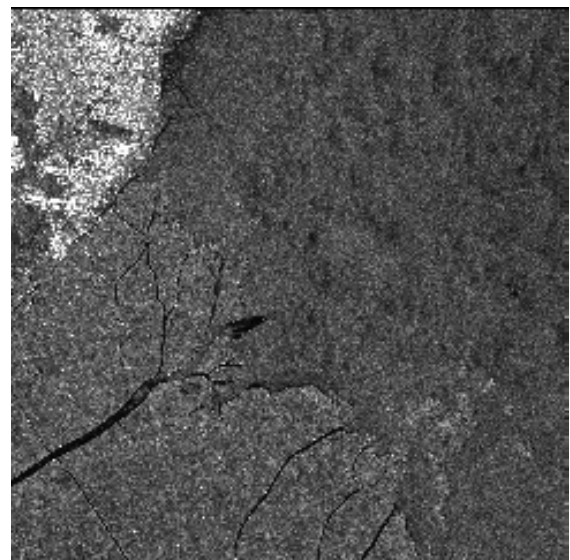
All the wavelet-based techniques used Daubechies 1 wavelet basis and 1 level of decomposition (improvements were not noticed with other basis of wavelets) [24], [25], [34].

Besides, Figure 7 summarizes the edge preservation performance of the POSAShrink technique vs. the rest of the shrinkage techniques with a considerably acceptable computational complexity.

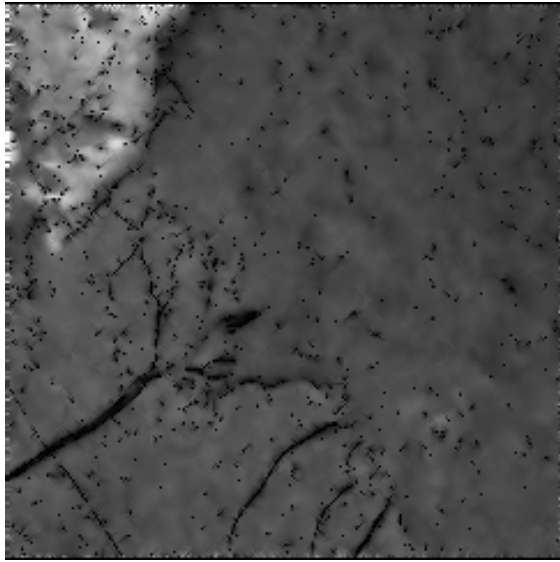
Table I shows the assessment parameters vs. 19 filters for figure. 7, where En-Lee means Enhanced Lee Filter, En-Frost means Enhanced Frost Filter, Non-log SWT means Non-logarithmic Stationary Wavelet Transform Shrinkage [27], Non-log DWT means Non-logarithmic DWT Shrinkage [28], VisuShrink (HT) means Hard-Thresholding, (ST) means Soft-Thresholding, and (SST) means Semi-ST [29]-[31].

The NMV and NSD are computed and compared over six different homogeneous regions in the choosed SAR image, before and after filtering, for all filters.

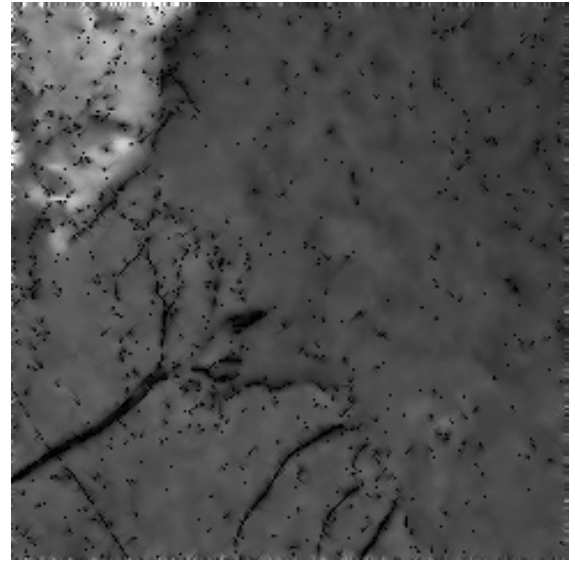
The POSAShrink has obtained the best mean preservation and variance reduction, as shown in Table I. Since a successful speckle reducing filter will not significantly affect the mean intensity within a homogeneous region, POSAShrink demonstrated to be the best in this sense too. The quantitative results of Table I show that the POSAShrink technique can eliminate speckle without distorting useful image information and without destroying the important image edges.



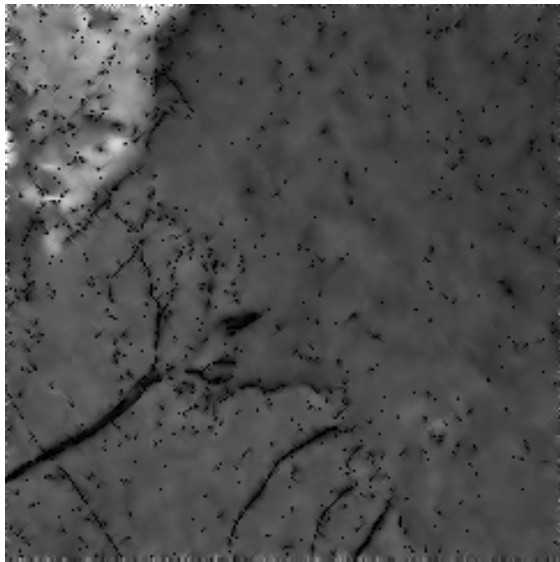
(a) Original



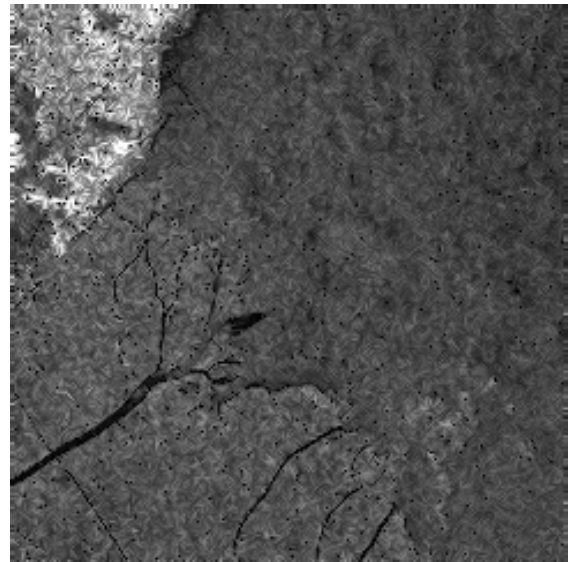
(b) VisuShrink



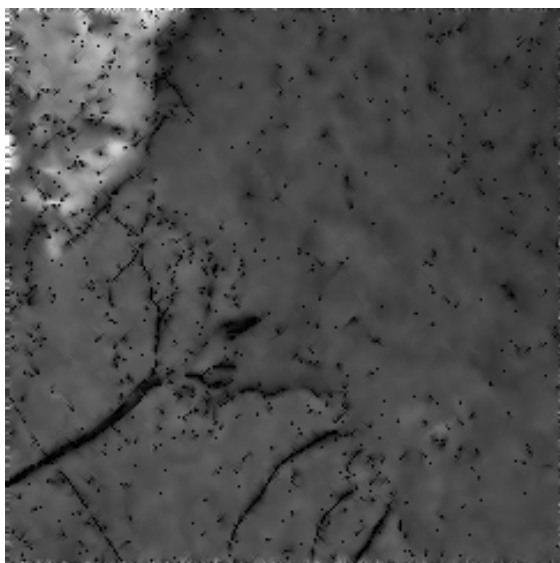
(e) SureShrink



(c) BayesShrink



(f) Our method



(d) OracleShrink

Fig. 7. (a) Original SAR image , (b,c,d,e) are results of some common ancient method, (f) result of our method.

Since we are interested in isolating the speckle noise in the image, the most appropriate wavelet function is one, which its shape looks like the speckle pattern. For this purpose, we computed the average of x and y cross sections of several speckle samples in the logarithmically transformed data. According to this study, the 2D Gaussian function has been found to be the best model fitted to the speckle pattern cross-section [35]-[39].

## VII. CONCLUSION

Direct smoothing of wavelet coefficient causes artificial structure, blurred and smoothed in image. By using SOM neural de-blurring algorithm, final image becomes more acceptable. Proportional to applying DWT, 15% improvement in edge prevention is received by new approach.

Although the SOM-based de-blurring 1) did not use the

traditional Gaussian neighborhood function as a property for the algorithm, 2) the learning-rate factor is constant along iterations, and 3) the width of the Kernel is constant along iterations too, the results are better than the results of such well-known methods as de-blurring. The drawback of this approach is complexity and time consuming. In one computer, our method long-time is 5 times as of DWT.

Further improvements to de-noising algorithm may be achieved using knowledge-based information such as image texture or PDF of radar cross section (RCS). Integrating these different kinds of information may be performed using Neural Networks. Finally, the natural extension of this work is in medical applications, as well as in micro arrays de-noising.

Table I shows the assessment parameters vs. 19 filters for Figure 5(a), where En-Lee means Enhanced Lee Filter, En-Frost means Enhanced Frost Filter, Non-log SWT means Non-logarithmic Stationary Wavelet Transform Shrinkage and Non-log DWT means Non-logarithmic DWT Shrinkage.

We compute and compare the NMV and NSD over six different homogeneous regions in our SAR image, before and after filtering, for all filters. The Smooth Shrink and de-blurring has obtained the best mean preservation and variance reduction, as shown in Table I. Since a successful speckle reducing filter will not significantly affect the mean intensity within a homogeneous region, Smooth Shrink and de-blurring demonstrated to be the best in this sense too. The quantitative results of Table I show that the Smooth Shrink technique can eliminate speckle without distorting useful image information and without destroying the important image edges. In fact, the Smooth Shrink outperformed the conventional and non conventional speckle reducing filters in terms of edge preservation measured by Pratt's figure of merit [34] [39], as shown in Table I.

TABLE I: ASSESSMENT PARAMETER AND FILTERS FOR FIGURE 5(A).

Filter	Assessment Parameter				
	MSD	NSD	ENL	DR	FOM
SAR image	-	43.996	11.093	2.558e	0.302
Kuan	542.73	40.836	16.962	3.267e	0.421
Median	614.74	42.5373	16.746	2.567e	0.400
Wiener	564.83	40.374	16.525	3.234e	0.442
DS	564.83	40.009	17.837	8.594e	0.457
EDS	564.83	40.009	17.424	8.986e	0.457
VisuShrink	855.30	32.868	39.088	7.861e	0.451
SureShrink	798.44	32.981	38.984	7.735e	0.452
OracleShrink	743.95	32.999	37.909	7.265e	0.452
BayesShrink	716.63	32.897	38.302	2.400e	0.452
Orcale Thr	732.23	33.312	36.846	6.735e	0.457
TNN	724.08	36.823	36.098	1.053e	0.458
SWT	300.28	43.827	11.228	1.578e	0.457
DWT	341.39	39.416	16.485	1.031e	0.458
DS	867.12	32.688	39.088	3.267e	0.459
Our method	871.31	31.701	39.900	3.294e	0.459

A Bayesian estimator was used for estimating the

de-noised wavelet coefficients. This estimator uses a priori knowledge on probability distribution of the signal and noise wavelet coefficients. This estimator performs like a feature detector, preserving the features that are clearly distinguishable in the speckled data such as lines and edges.

The whole algorithm is computationally expensive. Particularly, parameter estimation of the signal and noise distributions is the most time consuming part of the algorithm. More efficient parameter estimation algorithms may reduce the computational cost of this part. Further improvements to this algorithm may be achieved using knowledge-based information such as image texture or PDF of radar cross section (RCS). Integrating these different kinds of information may be performed using Neural Networks.

#### ACKNOWLEDGMENT

This work was supported in part by a grant from Islamic Azad University, Aharm Branch. Also, the authors wish to thank European DECLIMS project for real SAR images.

#### REFERENCES

- [1] H.S. Tan. De-noising of Noise Speckle in Radar Image. October, 2001.
- [2] S.G. Chang, B. Yu, and M. Vetterli, "Adaptive wavelet thresholding for image denoising and compression," IEEE Transactions on Image Processing, vol. 9, no. 9, pp.1532-1546, September 2000.
- [3] F. Argenti and L. Alparone, "Speckle removal from SAR images in the undecimated wavelet domain," IEEE Trans. Geosci. Remote Sensing, vol. 40, pp. 2363-2374, Nov. 2002.
- [4] L. Sendur and I. W. Selesnick, "A bivariate shrinkage function for wavelet-based denoising," in Proc. IEEE Int. Conf. Acoust., Speech, SignalProcessing (ICASSP), Orlando, May 13-17, 2002.
- [5] L. Sendur and I. W. Selesnick, "Bivariate shrinkage functions for wavelet-based denoising exploiting interscale dependency," IEEE Trans. Signal Processing, vol. 50, pp. 2744-2756, Nov. 2002.
- [6] L. Sendur and I. W. Selesnick, "Bivariate shrinkage with local variance estimation," IEEE Signal Processing Letters, vol. 9, pp. 438-441, Dec. 2002.
- [7] E. Simoncelli, "Statistical models for images: Compression, restoration and synthesis," in Proc. 31st Asilomar Conf. Signals, Syst., Comput., Nov. 1997, pp. 673-678.
- [8] V. Strela, J. Portilla, and E. Simoncelli, "Image de-noising using a local Gaussian scale mixture model in the wavelet domain," in Proc. SPIE 45<sup>th</sup> Annu. Meet., 2000.
- [9] Y. Yu, and S.T. Acton, "Speckle Reducing Anisotropic Diffusion," IEEE Trans. on Image Processing, vol. 11, no. 11, pp.1260-1270, 2002.
- [10] Alessandro Foi, Vladimir Katkovnik, and Karen Egiazarian, "Pointwise Shape-Adaptive DCT for High-Quality Denoising and Deblocking of Grayscale and Color Images," IEEE Transactions on Image Processing, vol. 16, no. 5, pp. 1395-1411, May 2007.
- [11] M. Mastriani and A. Giraldez, "Enhanced Directional Smoothing Algorithm for Edge- Preserving Smoothing of Synthetic-Aperture Radar Images," Journal of Measurement Science Review, vol 4, no. 3, pp.1-11, 2004.
- [12] M. Mastriani, "Denoising based on wavelets and deblurring via selforganizing map for Synthetic Aperture Radar images," ICGST International on Journal of Artificial Intelligence and Machine Learning, Volume 5, 2005.
- [13] M. Mastriani, "Fuzzy Thresholding in Wavelet Domain for Speckle education in Synthetic Aperture Radar Images," International Journal of Intelligent Technology, Volume 1, Number 3, pp.252-265, 2006.
- [14] S.Kother Mohideen, Dr. S. Arumuga Perumal, Dr. M.Mohamed Sathik, IJCSNS International Journal of Computer Science and Network Security, VOL.8 No.1, 2008.
- [15] H. Guo, J.E. Odegard, M. Lang, R.A. Gopinath, I. Selesnick, and C.S. Burrus, "Speckle reduction via wavelet shrinkage with application to SAR based ATD/R," Technical Report CML TR94-02, CML, Rice University, Houston, 1994.

- [16] D.L. Donoho and I.M. Johnstone, "Adapting to unknown smoothness via wavelet shrinkage," *Journal of the American Statistical Association*, vol. 90, no. 432, pp. 1200-1224, 1995.
- [17] S.G. Chang, B. Yu, and M. Vetterli, "Adaptive wavelet thresholding for image denoising and compression," *IEEE Transactions on Image Processing*, vol. 9, no. 9, pp.1532-1546, September 2000.
- [18] X.-P. Zhang, "Thresholding Neural Network for Adaptive Noise reduction," *IEEE Transactions on Neural Networks*, vol.12, no. 3, pp.567-584, May 2001.
- [19] N. K. Bose and S. Lertrattanapanich. *Advances in wavelet superresolution*. [Online]. Available: <http://www.personal.psu.edu/users/s/x/sxl46/Bose01w.pdf>
- [20] S. P. Kim and N. K. Bose, "Reconstruction of 2-D bandlimited discrete signals from nonuniform samples," *IEE Proceedings*, Vol.137, No.3, Part F, June 1990, pp. 197-203.
- [21] Seunghyeon Rhee and Moon Gi Kang, "Discrete cosine transform based regularized high-resolution image reconstruction algorithm," *Optical Engineering*, Vol.38, No.8, 1999, pp. 1348-1356.
- [22] S. P. Kim, N. K. Bose and H. M. Valenzuela, "Recursive reconstruction of high resolution image from noisy undersampled multiframe," *IEEE Trans. on Acoust., Speech, and Signal Process.*, Vol.38, 1990, pp. 1013-1027.
- [23] C. Ford and D. Etter, "Wavelet basis reconstruction of nonuniformly sampled data," *IEEE Trans. Circuits and System II*, Vol.45, No.8, August 1998, pp.1165-1168.
- [24] N. Nguyen and P. Milanfar, "A wavelet-based interpolation-restoration method for superresolution (wavelet superresolution)," *Circuits Systems and Signal Process*, Vol.19, No.4, 2000, pp.321-338.
- [25] F. Argenti and L. Alparone, "Speckle removal from SAR images in the undecimated wavelet domain," *IEEE Trans. Geosci. Remote Sensing*, vol. 40, pp. 2363-2374, Nov. 2002.
- [26] H. Xie, L. E. Pierce, and F. T. Ulaby, "Statistical properties of logarithmically transformed speckle," *IEEE Trans. Geosci. Remote Sensing*, vol. 40, pp. 721-727, Mar. 2002.
- [27] J.W. Goodman, "Some fundamental properties of speckle," *Journal Optics Society of America*, 66:1145-1150, 1976.
- [28] S.J. Leon, *Linear Algebra with Applications*, Maxwell Macmillan International Editions, New York, 1990.
- [29] G.G. Walter, "Sampling Theorems and Wavelets," in *Handbook of Statistics*, Vol. 10, (eds. N.K. Bose and C.R. Rao), Elsevier Science Publishers B.V., North-Holland, Amsterdam, The Netherlands, 1993, pp. 883-903.
- [30] M. Vetterli and J. Kovacevic, "Wavelets and Subband Coding," Prentice Hall PTR, Upper Saddle River, New Jersey 07458, 1995.
- [31] S. Mann and R.W. Picard, "Video orbits of the projective group: A simple approach to featureless estimation of parameters," *IEEE Transactions on Image Processing*, Vol. 6, No.9, September 1997, pp.1281-1295.
- [32] Abrishami Moghaddam, H., Valadan Zouj, M.J., Dehghani, M., 2004. Bayesian-based speckle reduction using wavelet transforms. Accepted in the Conference on Applications of Digital Image Processing in 49th SPIE annual meeting, Denver, CO USA
- [33] Achim, A., Bezerianos, A. and Tsakalides, P., 2001. Novel Bayesian Multiscale for speckle Removal in Medical Ultrasound Images, *IEEE Trans. Med. Imaging Journal*, 20(8), pp. 772-783.
- [34] Fodor, I. K., Kamath, C., 2003. Denoising Through Wavelet Shrinkage: An Empirical Study, *Journal of Electronic Imaging*, 12, pp.151-160.
- [35] Gose, E., Johnsonbaugh, R. and Jost, S., 1996. *Pattern Recognition and Image Analysis*, Prentice Hall, Inc., USA.
- [36] Leon-Garcia, A., 1994. *Probability and Random Processes for Electrical Engineering*, Addison-Wesley Inc.
- [37] Li, C., 1987. Two Adaptive Filters for Speckle Reduction in SAR Imagery by Using the Variance Ratio, *International Journal of Remote Sensing*, 9(4), pp. 641-653.
- [38] Lopes, A., Touzi, R. and Nesry, E., 1990. Adaptive speckle filter and scene heterogeneity, *IEEE Trans. on Geoscience and Remote Sensing Journal*, 28, pp. 992-1000.
- [39] Nunez, J., Otazu, X., Fors, O., Prades, A., Pala, V. and Arbiol, R. 1999. Multiresolution-based Image Fusion with Additive Wavelet Decomposition, *IEEE Trans. Geoscience and Remote Sensing Journal*, 37(3), pp. 1204-1211.



**Ashkan Masoomi** was born in Boushehr, Iran at 1983. He got Diploma in Physics and Mathematics in 2003. He continues his study in Department of Electronic and Communication Engineering, Islamic Azad University of Boushehr, Iran. Now He has M.Sc. in communication Engineering and B.Sc. in Electronic Engineering. His Final Thesis was "De-speckling and Ship Detection in SAR Images". His Research Interests are: Satellite communication, Security information, Signal and Image Processing, Image de-noising and Compression, Remote sensing, Shape detection, robotics and RF MEMES. Also he works in Aerospace Researches Institute of Islamic Azad University, Boushehr branch, Iran. He published 2 papers in ISI journal, 4 papers in international journal, 8 papers in IEEE conference and 4 papers in international conference. He was one of chair session in ICMAE2011 international conference in Thailand.



**Roozbeh Hamzehyan** was born in Shiraz, Iran in 1982. He received the B.Sc. degree in Electronics Engineering from Islamic Azad University of Bushehr, Iran in 2004, M.Sc. Degree in communication engineering from Bushehr University in 2008. He has authored more than 12 published technical papers in communication and electronics. His current research activities include Detection, RF Integrated Circuit design and Satellite communication.

**Najmeh Charaghi Shirazi** was born in Shiraz, Iran in 1982. She is a student of PhD in Electronic Engineering Tehran science and research branch. She received the B.Sc. and M.Sc. degree in Electronics Engineering from Islamic Azad University, Bushehr branch, Iran in 2005 and 2009. She has authored more than 10 published technical papers in electronics. Her current research activities include analog circuit and RF Integrated Circuit design and Satellite communication.